THE JOURNAL OF BIOLOGICAL CHEMISTRY VOL. 280, NO. 37, pp. 32061–32068, September 16, 2005
Printed in the U.S.A.

Myosin VIIB from *Drosophila* Is a High Duty Ratio Motor*

Received for publication, June 21, 2005, and in revised form, July 22, 2005 Published, JBC Papers in Press, July 29, 2005, DOI 10.1074/jbc.M506765200

Yi Yang[1], **Mihály Kovács**[1], **Qian Xu, John B. Anderson, and James R. Sellers**[2]

From the Laboratory of Molecular Physiology, NHLBI, National Institutes of Health, Bethesda, Maryland 20892-1762

Myosin VII is an unconventional myosin widely expressed in organisms ranging from amoebae to mammals that has been shown to play vital roles in cell adhesion and phagocytosis. Here we present the first study of the mechanism of action of a myosin VII isoform. We have expressed a truncated single-headed *Drosophila* myosin VIIB construct in the baculovirus-Sf9 system that bound calmodulin light chains. By using steady-state and transient kinetic methods, we showed that myosin VIIB exhibits a fast release of phosphate and a slower, rate-limiting ADP release from actomyosin. As a result, myosin VIIB will be predominantly strongly bound to actin during steady-state ATP hydrolysis (its duty ratio will be at least 80%). This kinetic pattern is in many respects similar to that of the single-molecule vesicle transporters myosin V and VI. The enzymatic properties of myosin VIIB provide a kinetic basis for processivity upon possible dimerization via the C-terminal domains of the heavy chain. Our experiments also revealed conformational heterogeneity of the actomyosin VIIB complex in the absence of nucleotide.

Myosins constitute a diverse superfamily of actin-based motors consisting of at least 19 classes (1). Myosins from class VII have been shown to be expressed in various organisms including *Dictyostelium*, *Caenorhabditis*, *Drosophila*, mouse, and humans (2–6). Myosin VII isoforms have been implicated to play vital roles in cell adhesion and phagocytosis (7, 8). In mammals there are two myosin VII genes termed VIIA and VIIB. Mutations of myosin VIIA in humans are responsible for Usher syndrome type 1B characterized by hearing impairment and retinitis pigmentosa (9, 10). In mice, myosin VIIA mutants (*shaker-1*) exhibit severe sensory dysfunction because of disorganization of the stereocilial bundle of auditory hair cells (3). Lack of myosin VIIA activity in *Drosophila* crinkled (*ck*) mutants results in deafness or embryonic/larval lethality (5, 11). Based on motor domain sequence analysis, the fly myosin VIIs form a distinct phylogenetic cluster from the group of mammalian myosin VIIs, and thus *Drosophila* myosins VIIA and VIIB are not orthologous to their mammalian counterparts (12). On the other hand, loss of myosin VIIA function causes deafness in both *Drosophila* and mammals (3, 9–11).

As in most other myosins, the myosin VII heavy chain consists of an N-terminal motor domain containing the actin and ATP-binding sites, a neck (light chain-binding) domain, and a C-terminal tail consisting of several effector domains. The tail of myosin VII comprises a putative coiled-coil region, two MyTH4 and FERM domains, and a Src homology 3 domain. These domains interact with various binding partners of effector function. One of the identified binding partners is MyRIP (myosin VIIA- and Rab-interacting protein) that associates with the myosin VIIA tail domain and Rab27A to connect retinal melanosomes to the actin cytoskeleton and regulate their trafficking (13). Another binding partner is vezatin, which can interact with both the myosin VIIA C-terminal FERM domain and the cadherin-catenin complex and thus create a link between adherens junctions and the actin cytoskeleton and strengthen cell-cell adhesion (14). Talin has recently been shown to associate directly with myosin VII in *Dictyostelium*, thus mediating cell-substrate adhesion and filopodial extension (6, 14). These data indicate a role for myosin VII in organelle transport and the maintenance of contact and/or tension between the actin cytoskeleton and the cell membrane.

Although two mammalian myosin VIIA orthologs have been shown to exhibit actin-activated ATPase activity and *in vitro* motility (15, 16), no detailed mechanistic study has been performed on any myosin VII isoform. In the present paper, we report an in-depth biochemical kinetic characterization of a recombinant single-headed *Drosophila* myosin VIIB construct (mVIIB-S1). We demonstrate that this myosin uses a kinetic mechanism characterized by a high actin attachment ratio during rapid ATPase cycling. These properties are mainly defined by the kinetics of sequential product release steps (fast phosphate release and rate-limiting ADP dissociation). These features, which are similar to those of myosin V and VI, will be of central importance in the tension-bearing and/or possible processive transport role of myosin VII in cells.

EXPERIMENTAL PROCEDURES

Expression and Purification of the Myosin VIIB-S1 (mVIIB-S1) Protein—A cDNA fragment encoding the first 842 amino acids (motor domain plus all five predicted light chain-binding IQ motifs) of the *Drosophila* myosin VIIB heavy chain (Myo28B1) was amplified from an earlier *Drosophila* myosin VIIB clone (12) and subcloned into baculovirus transfer vector pFastBac1 (Invitrogen). The complete nucleotide sequence of the recombinant plasmid was confirmed by double-stranded DNA sequencing. A FLAG tag (DYKDDDDK) was fused to the C terminus of mVIIB-S1 to aid purification. mVIIB-S1 was co-expressed with *Drosophila* calmodulin in Sf9 cells. The expressed mVIIB-S1 protein was purified as described previously for non-muscle myosin IIA heavy meromyosin (17).

Kinetic Measurements—Steady-state ATPase activities were measured by an NADH-coupled assay at 25 °C as described previously (18) in the presence of 10 mM MOPS[3] (pH 7.0), 2 mM $MgCl_2$, 0.15 mM EGTA, 1 mM ATP, and 10 mM KCl. Stopped-flow measurements were performed using a KinTek SF-2001 stopped-flow instrument (KinTek Corp., Austin, TX) at 25 °C in a buffer containing 20 mM MOPS (pH 7.0), 5 mM $MgCl_2$, 0.05 mM EGTA, and 50 mM KCl (10 mM KCl was used in stopped-flow experiments measuring P_i release). Optical setups were as described previously (19). Quenched-flow experiments were carried out using a KinTek RQF-3 quenched-flow instrument as described earlier (18) except that 1 M HCl was used as a chemical quench instead of

* The costs of publication of this article were defrayed in part by the payment of page charges. This article must therefore be hereby marked "*advertisement*" in accordance with 18 U.S.C. Section 1734 solely to indicate this fact.

[1] Both authors contributed equally to this work.

[2] To whom correspondence should be addressed: Laboratory of Molecular Physiology, NHLBI, Bldg. 10, Rm. 8N202, National Institutes of Health, Bethesda, MD 20892-1762. Tel.: 301-496-6887; Fax: 301-402-1542; E-mail: sellersj@nhlbi.nih.gov.

[3] The abbreviations used are: MOPS, 4-morpholinepropanesulfonic acid; dm, 2′-deoxy-methylanthranyloyl-; PBP, phosphate-binding protein; MDCC, *N*-[2-(1-maleimidyl)-ethyl]-7-(diethylamino)coumarin-3-carboxamide.

trichloroacetic acid. Reagent concentrations stated in rapid mixing experiments refer to post-mix concentrations unless stated otherwise.

Actin from rabbit skeletal muscle was prepared (20) and pyrene-labeled (21) as described. Actin filaments were stabilized by a 1.5-fold molar excess of phalloidin (Calbiochem) in all experiments. mVIIB-S1 and acto-mVIIB-S1 were made nucleotide-free by preincubation with 0.02 units/ml apyrase for 30 min at 25 °C when required. 2′-Deoxy-methylanthranyloyl-ATP and -ADP (dmATP and dmADP, respectively) and fluorescently labeled bacterial phosphate-binding protein (MDCC-PBP) (22) were generously provided by Dr. Howard White (Eastern Virginia Medical School). Other reagents were from Sigma.

Means ± S.D. are reported for 2–3 rounds of experiments. Data fitting and analysis was done using the KinTek SF-2001 software and OriginLab 7.0 (Microcal Corp.).

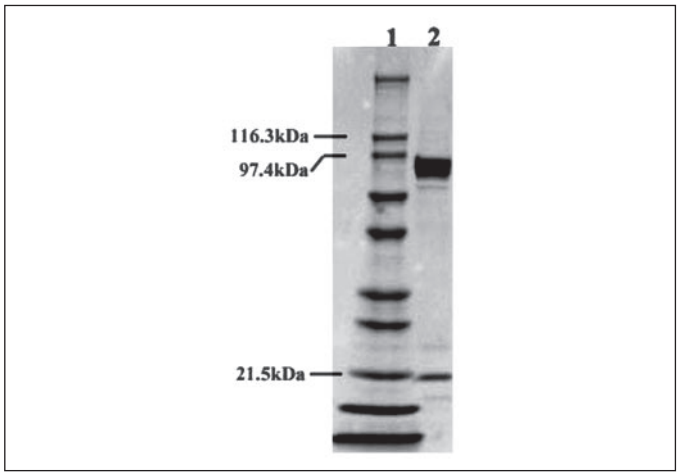

FIGURE 1. **SDS-polyacrylamide electrophoretogram of mVIIB-S1.** Samples were run on a 4–20% gradient polyacrylamide-SDS gel. *Lane 1*, Molecular weight marker. *Lane 2*, FLAG-affinity purified mVIIB-S1 consisting of a 99-kDa heavy chain and 17-kDa calmodulin light chains.

RESULTS

Construct Design and Expression—The mVIIB-S1 heavy chain construct we used contains the motor domain and the entire neck region of *Drosophila* myosin VIIB, up to the beginning of the predicted coiled-coil segment. We co-expressed the mVIIB-S1 heavy chain with *Drosophila* calmodulin, because bovine myosin VIIA has been shown previously to bind calmodulin in immunoprecipitation experiments (16). The mVIIB-S1 construct showed reasonably good levels of expression in the baculovirus-Sf9 system, and generally 1 mg of protein could be purified from 10^9 cells.

Previously, we identified the presence of five putative light chain-binding IQ motifs in the neck region of *Drosophila* myosin VIIB (12). Most interestingly, the relative intensities of the heavy chain and calmodulin bands in the electrophoretic profile of purified mVIIB-S1 indicated that calmodulins bind in a smaller number to the heavy chain (Fig. 1).

ATPase Mechanism in the Absence of Actin—We used 2′-deoxy-mant-ATP (dmATP), a fluorescent ATP analog, to monitor the kinetics of ATP binding to mVIIB-S1. When mixed with mVIIB-S1 in the stopped-flow apparatus under pseudo-first-order conditions, dmATP showed a single exponential fluorescence increase on binding to the protein (Fig. 2*A*, *inset*). The second-order binding rate constant calculated from the linear slope of the plot of the observed rate constant (k_{obs}) *versus* [dmATP] was 3.4 ± 0.1 $\mu M^{-1}\,s^{-1}$ (Fig. 2*A*). (The kinetic frame-

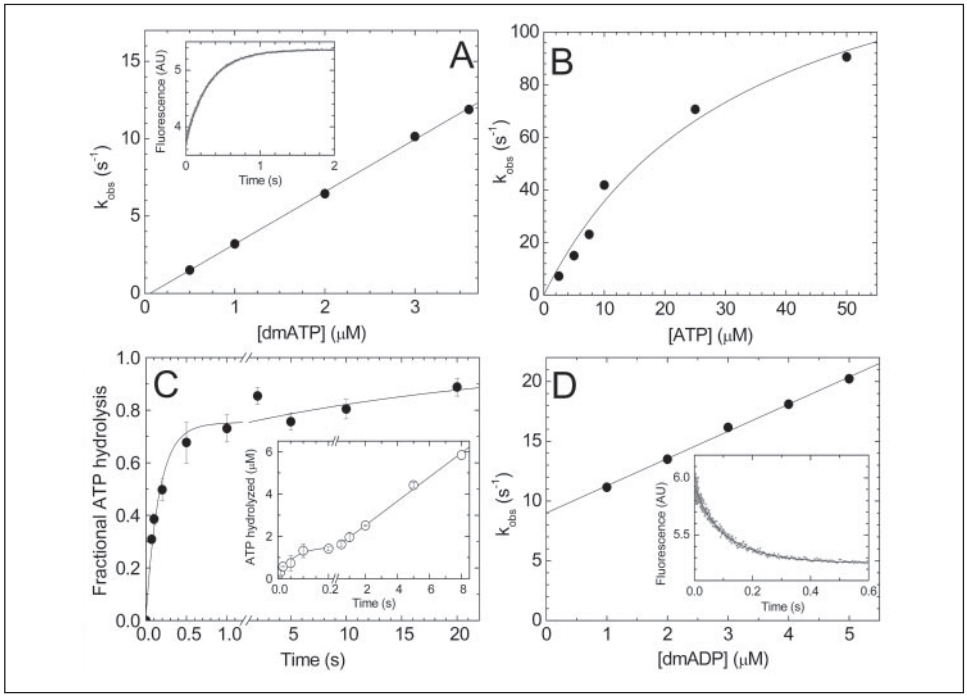

FIGURE 2. **Transient kinetics of mVIIB-S1 in the absence of actin.** *A*, observed rate constants (k_{obs}) of single exponential dmATP fluorescence transients on mixing 0.2 μM mVIIB-S1 with the indicated dmATP concentrations in the stopped-flow apparatus. A linear fit of the data set yielded a second-order binding rate constant (K_1k_2 in Scheme 1) of 3.4 ± 0.1 $\mu M^{-1}\,s^{-1}$. The *inset* shows a trace at 1 μM dmATP that had a k_{obs} of 3.2 s^{-1}. *B*, k_{obs} values of single exponential tryptophan fluorescence transients recorded upon mixing 1 μM mVIIB-S1 with the indicated ATP concentrations. k_{obs} showed a hyperbolic dependence on ATP concentration with a maximum ($k_3 + k_{-3}$) of 160 ± 30 s^{-1} and half-saturation occurring at 34 ± 10 μM ATP. *C*, time course of ATP hydrolysis upon mixing 2.9 μM mVIIB-S1 with 1.5 μM ATP in the quenched-flow apparatus (single turnover conditions). A double exponential approximation to the reaction time course indicated that the initial fast phase (the so-called P_i burst) had a fractional amplitude of 0.74 (k_{obs} = 6.2 s^{-1}), followed by a slower phase rate-limited by P_i release. *Inset*, Time course of ATP hydrolysis on mixing 2.9 μM mVIIB-S1 with 25 μM ATP (multiple turnover experiment). The time course consisted of an exponential burst phase with an amplitude of 1.4 μM (corresponding to 0.48 mol P_i/mol mVIIB-S1) and a k_{obs} of 18 s^{-1}, which was followed by a linear steady-state phase with a slope of 0.20 s^{-1}. *D*, k_{obs} values of single exponential dmADP fluorescence transients on rapidly mixing 0.2 μM mVIIB-S1 with the indicated dmADP concentrations. A linear fit of the data yielded a second-order binding rate constant (k_{-5}) of 2.3 ± 0.1 $\mu M^{-1}\,s^{-1}$. The intercept of the plot delineated an off-rate constant (k_5) of 9.0 ± 0.2 s^{-1}. The *inset* shows the results of a chasing experiment in which a pre-mixture of 0.5 μM mVIIB-S1 and 5 μM dmADP was rapidly mixed with excess (1 mM) ATP in the stopped-flow. The trace shown had a k_{obs} (= k_5) of 10.7 s^{-1}. Conditions: 25 °C, 20 mM MOPS (pH 7.0), 5 mM $MgCl_2$, 50 mM KCl, 0.05 mM EGTA.

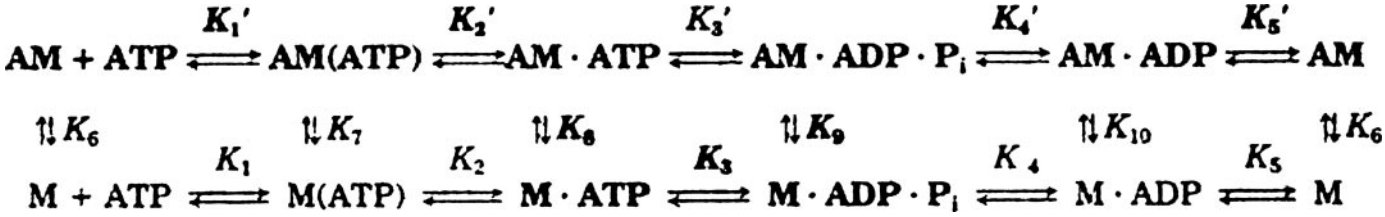

SCHEME 1. The symbols used are as follows: *A*, actin; *M*, myosin. Equilibrium constants are expressed in rightward or downward directions. *Arrows* for associating or dissociating components are omitted for clarity.

TABLE ONE

Kinetic parameters of the mVIIB-S1 ATPase cycle with corresponding values for myosins Va and VI

Numbering of steps refers to Scheme 1.

	Signal or calculation	mVIIB-S1[a]	Myosin Va[b]	Myosin VI[c]
Steady-state ATPase activity				
k_{basal} (s^{-1})	NADH assay	0.020	0.03	0.04
V_{max} (s^{-1})	NADH assay	8.4 ± 0.6	15	8.3
K_{ATPase} (μM)	NADH assay	39 ± 5	1.4	2.8
Actin binding				
k_{-6} ($\mu M^{-1}s^{-1}$)	Pyrene-actin	1.2 ± 0.1	73	5.4
k_6 (s^{-1})	Pyrene-actin	0.042	0.00036	0.005
K_6 (μM)	k_6/k_{-6}	0.035	0.0000049	0.0009
k_{-10} ($\mu M^{-1}s^{-1}$)	Pyrene-actin	1.0 ± 0.1	4.2	2.0
k_{10} (s^{-1})	Pyrene-actin	0.034	0.032	0.06
K_{10} (μM)	k_{10}/k_{-10}	0.034	0.0076	0.067
K_9 (μM)	MDCC-PBP	>30	9[d]	32
ATP binding[e]				
K_1k_2 ($\mu M^{-1}s^{-1}$)	dmATP	3.4 ± 0.1	1.6	0.24
	Tryptophan	4.7		
$K_1'k_2'$ ($\mu M^{-1}s^{-1}$)		[e]	0.9	0.015
k_2' (s^{-1})		[e]	≥750	>250
ATP hydrolysis				
$k_3 + k_{-3}$ (s^{-1})	Tryptophan	160 ± 30	750	
K_3	Quenched-flow	2.8	>9	≥1.4
P_i release				
k_4 (s^{-1})	$k_{basal}(1 + K_3)/K_3$	0.027	0.03	0.04
k_4' (s^{-1})	MDCC-PBP	>40	110[d]	89
k_4'/K_9' ($\mu M^{-1}s^{-1}$)	MDCC-PBP	0.79	12	2.8
ADP binding				
k_5 (s^{-1})	dmADP	9.0 ± 0.2	1.2	6.4
k_{-5} ($\mu M^{-1}s^{-1}$)	dmADP	2.3 ± 0.1	4.6	1.06
K_5 (μM)	k_5/k_{-5}	3.8	0.27	6.0
k_5' (s^{-1})	dmADP chase	9.6 ± 1.3	12	5.6
	dmADP intercept	16 ± 1		
	Pyrene-actin	9.8 ± 3.5		
k_{-5}' ($\mu M^{-1}s^{-1}$)	dmADP	2.7 ± 0.4	12.6	0.60
	k_5'/K_5' (pyrene-actin data)	5.8		
K_5' (μM)	k_5'/k_{-5}' (dmADP data)	3.6–5.9	0.8	8.8
	dmADP amplitudes	2.7 ± 0.4		
	Pyrene-actin	1.7 ± 0.9		
Actin-ADP coupling				
K_5'/K_5	dmADP	0.7–1.6	3.0	1.5
K_{10}/K_6	Pyrene-actin	0.97	1550	74
k_5'/k_5	dmADP	1.1–1.8	10	0.88

[a] Data refer to this study.
[b] Data refer to Ref. 29 unless otherwise stated.
[c] Data refer to Ref. 30; T406E point mutant mimicking the heavy chain-phosphorylated form.
[d] Data refer to Ref. 41.
[e] See Table II for parameters.

TABLE TWO

Parameters of the two phases of ATP-induced acto-mVIIB-S1 dissociation

	Phase 1	Phase 2
Pyrene-actin		
$K_1'k_2'$ ($\mu M^{-1}s^{-1}$)	1.3 ± 0.1	0.31 ± 0.08
k_2' (s^{-1})	>400	>50
Fractional amplitude[a]	0.56 ± 0.15	0.44 ± 0.15
dmATP		
$K_1'k_2'$ ($\mu M^{-1}s^{-1}$)	2.2 ± 0.1	0.46 ± 0.02
Fractional amplitude	0.46 ± 0.06	0.54 ± 0.06

[a] With the omission of the third ATP concentration-independent phase.

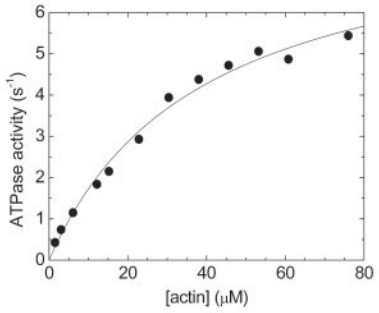

FIGURE 3. **Steady-state actin-activated ATPase activity of mVIIB-S1.** The ATPase activity of acto-mVIIB-S1 depended hyperbolically on actin concentration showing a V_{max} of 8.4 ± 0.6 s^{-1} and a K_{ATPase} (actin concentration at half-maximal activation) of 39 ± 5 μM. Conditions: 25 °C, 10 mM MOPS (pH 7.0), 2 mM $MgCl_2$, 0.15 mM EGTA, 1 mM ATP, 10 mM KCl.

work used for the actomyosin ATPase cycle is shown in Scheme 1. TABLES ONE and TWO summarize all parameters measured in this study.)

Similarly to other myosins (23–25), mVIIB-S1 showed an increase in tryptophan fluorescence on interacting with ATP. The tryptophan fluorescence increase occurs upon a protein isomerization occurring on nucleotide binding (k_2 in Scheme 1) and/or on the ATP hydrolysis step ($k_3 + k_{-3}$). The maximal k_{obs} likely reflects the kinetics of the ATP hydrolysis step ($k_3 + k_{-3}$), with possible contributions from k_2. The tryptophan fluorescence increase transients were single exponential, and their k_{obs} showed saturation around 160 s^{-1} (Fig. 2*B*). The second-order ATP-binding rate constant (K_1k_2 in Scheme 1) deduced from the parameters of the hyperbolic fit of Fig. 2*B* ($K_1k_2 = k_{obs,\,max}/K_{½}$ where $K_{½}$ is the ATP concentration at half-maximal k_{obs} value) was 4.7 μM^{-1} s^{-1}.

To monitor directly ATP hydrolysis in the transient state, we performed quenched-flow experiments with mVIIB-S1. When mVIIB-S1 was rapidly mixed with a substoichiometric amount of [γ-^{32}P]ATP (single turnover conditions), the time course of ATP hydrolysis consisted of two phases (Fig. 2*C*). ATP hydrolysis in the fast phase was rate-limited by ATP binding. The fractional amplitude of this phase (A_{fast} = 0.74) reflects the equilibrium constant of the ATP hydrolysis step ($K_3 = A_{fast}/(1 - A_{fast})$ = 2.8), which rapidly equilibrates after ATP binding. The subsequent slow and irreversible release of phosphate in the second phase (k_4) completes the reaction (Fig. 2*C*). The value thus obtained for K_3 is likely to represent a lower limit for the equilibrium constant, because the second phase was difficult to resolve accurately. In a multiple turnover experiment in which mVIIB-S1 was mixed with excess ATP, an exponential P_i burst of 0.48 mol of P_i/mol of S1 was observed, which was followed by a linear phase of steady-state ATP hydrolysis (Fig. 2*C, inset*). The lower burst than that in the single turnover measurement may result from the fact that the multiple turnover experiment is influenced by uncertainties in protein concentration determination and/or the presence of a minor inactive subpopulation in the mVIIB-S1 preparation.

We monitored the interaction of mVIIB-S1 with ADP using dmADP, a fluorescent nucleotide analog. Upon mixing mVIIB-S1 with excess dmADP in the stopped-flow, single exponential traces were observed as dmADP fluorescence increased on binding to mVIIB-S1. The dependence of k_{obs} on dmADP concentration was linear in the observed range (Fig. 2*D*). The slope of the plot yielded a second-order binding rate constant (k_{-5}) of 2.3 ± 0.1 μM^{-1} s^{-1}, and the intercept delineated an off-rate constant (k_5) of 9.0 ± 0.2 s^{-1}. The off-rate constant was confirmed in chasing experiments in which the complex of mVIIB-S1 with dmADP was mixed with a large excess of ATP in the stopped-flow (Fig. 2*D, inset*). These experiments yielded a k_5 of 10.1 ± 0.7 s^{-1}.

Because all measured steps of the basal mVIIB-S1 ATPase cycle (ATP binding, hydrolysis, and ADP release) appear to be much faster than the measured basal steady-state ATPase rate (0.020 s^{-1} measured in a NADH-coupled steady-state assay), it is likely that the latter is limited largely by the phosphate release step (k_4), as is the case in all myosins examined.

Actin Activation of the Steady-state ATPase Activity—The steady-state ATPase activity of mVIIB-S1 was activated by actin to a maximum (V_{max}) of 8.4 ± 0.6 s^{-1} (Fig. 3 and TABLE ONE). The actin concentration required for half-maximal activation (K_{ATPase}) was 39 ± 5 μM. Note that these steady-state measurements were done in 10 mM KCl instead of 50 mM KCl applied in most transient kinetic experiments of the present study.

Actin Binding in the Absence of Nucleotide and in ADP—Actin site-specifically labeled with pyrene has been used extensively to monitor the strong binding interaction of myosin with actin in the case of many myosins (26, 27). Pyrene-actin showed a large (>50%) fluorescence quench on binding to mVIIB-S1, which we could exploit in measuring the actin binding kinetics of mVIIB-S1 by mixing mVIIB-S1 or mVIIB-S1·ADP with pyrene-actin under pseudo-first-order conditions in the stopped-flow (Fig. 4*A, inset*). Fig. 4*A* shows the dependence of the k_{obs} of the observed fluorescence quench on pyrene-actin concentration. The slopes of the plots delineate second-order actin binding rate constants of 1.2 ± 0.1 and 1.0 ± 0.1 μM^{-1} s^{-1} in the absence of nucleotide (k_{-6}) and in ADP (k_{-10}), respectively.

The rate constant of mVIIB-S1 dissociation from actin is expected to be low and therefore cannot be accurately determined from the intercepts of the plots of Fig. 4*A*. Thus, we performed chasing experiments in which the pyrene-acto-S1 rigor complex or the pyrene-acto-S1·ADP ternary complex was rapidly mixed with excess unlabeled actin in the stopped-flow. Fig. 4*B* shows the obtained pyrene fluorescence transients. Single exponential fits to the transients revealed dissociation rate constants from actin of 0.042 and 0.034 s^{-1}, respectively, for S1 (k_6) and S1·ADP (k_{10}). Single exponential fits showed some systematic deviation from the traces (Fig. 4*B*). Although the introduction of an additional phase slightly improved the fits (data not shown), the k_{obs} values of the two phases were only separated by factors of 3–4 and thus may not bear practical significance. Therefore, we believe that the reported single exponential rate constants represent reasonably good estimates for the dissociation rate constants. These results demonstrate that the presence of ADP does not notably affect the kinetics of actin binding and release.

Interaction of Acto-mVIIB-S1 with Nucleotides—We followed the kinetics of ATP-induced dissociation of the pyrene-acto-mVIIB-S1 complex in stopped-flow experiments in which pyrene-acto-mVIIB-S1 was mixed with increasing concentrations of ATP under pseudo-first-order conditions. Most interestingly, the traces were clearly triphasic throughout the ATP concentration range examined, which is a more complicated behavior than that observed with other myosins (Fig. 5*A*,

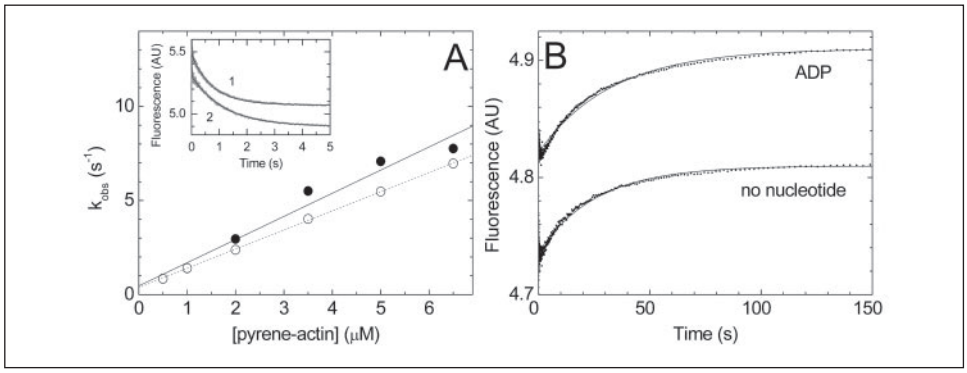

FIGURE 4. **Actin interaction of mVIIB-S1 in the absence of nucleotide and in ADP.** *A*, k_{obs} values of pyrene fluorescence transients recorded on rapidly mixing 0.2 μM mVIIB-S1 with pyrene-actin at the indicated concentrations in the absence of nucleotide (*solid symbols*) and in the presence of 10 μM ADP (*open symbols*). Linear fits to the data sets yielded second-order actin binding rate constants of 1.2 ± 0.1 μM^{-1} s^{-1} (k_{-6}) and 1.0 ± 0.1 μM^{-1} s^{-1} (k_{-10}) in the absence of nucleotide and in ADP, respectively. The *inset* shows records at 1 μM pyrene-actin (*trace 1*, no nucleotide, k_{obs} = 1.3 s^{-1}; *trace 2*, in ADP, k_{obs} = 1.2 s^{-1}). Traces are offset for clarity. Traces contained a minor fast phase with a k_{obs} of around 100 s^{-1} that did not show actin concentration dependence and therefore we attribute it to a mixing artifact. *B*, pyrene fluorescence records obtained on mixing a pre-mixture of 0.15 μM mVIIB-S1 and 0.4 μM pyrene-actin with 5 μM unlabeled actin in the stopped-flow in the absence of nucleotide and in 10 μM ADP (in both syringes). Single exponential fits to the transients yielded dissociation rate constants of mVIIB-S1 from pyrene-actin of 0.042 s^{-1} (k_6, no nucleotide) and 0.034 s^{-1} (k_{10}, in ADP). Traces are offset for clarity. Conditions were as in Fig. 2.

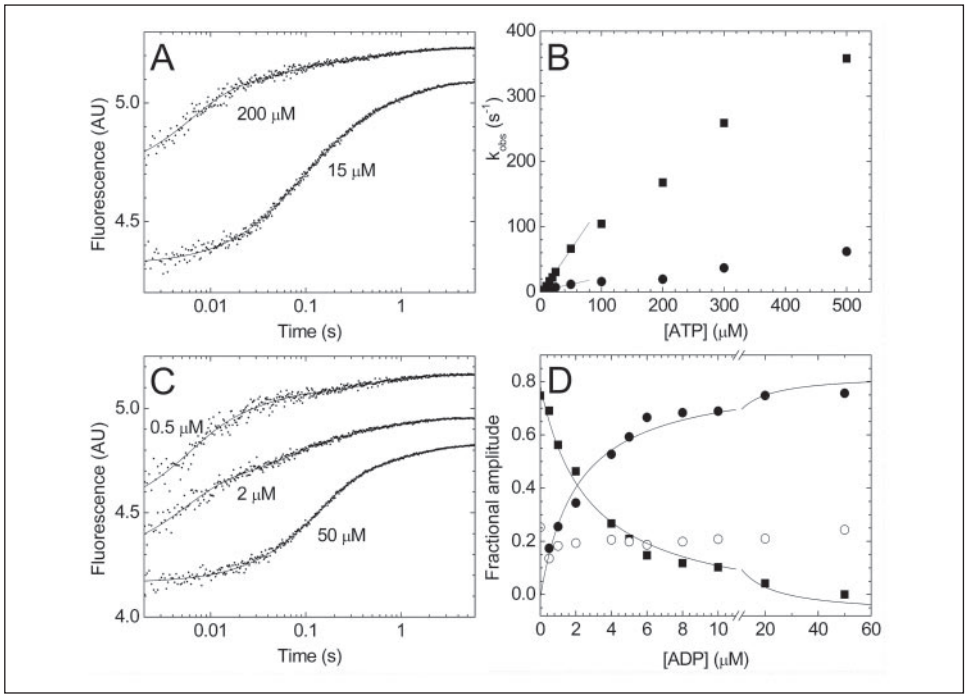

FIGURE 5. **Interaction of acto-mVIIB-S1 with ATP and ADP.** *A*, pyrene fluorescence transients recorded upon mixing a pre-mixture of 0.5 μM pyrene-actin and 0.25 μM mVIIB-S1 with the indicated ATP concentrations. The transients were fitted by three exponentials. Fitted rate constants of the phases are as follows: at 15 μM ATP, 16 s^{-1} (49% fractional amplitude), 4.3 s^{-1} (38%), and 0.78 s^{-1} (20%); at 200 μM ATP, 170 s^{-1} (59%), 19 s^{-1} (25%), and 1.3 s^{-1} (16%). Traces are offset for clarity. *B*, dependence of the k_{obs} values of the first (*squares*) and second (*circles*) phases in the experiments of Fig. 5*A* on ATP concentration. Linear fits to the data points at low [ATP] yielded slopes ($K_1'k_2'$) of 1.4 and 0.22 μM^{-1} s^{-1}, respectively, for the first and second phases in the experiment shown. *C*, pyrene fluorescence records obtained on mixing a pre-mixture of 0.5 μM pyrene-actin, 0.25 μM mVIIB-S1, and the indicated ADP concentrations with 500 μM ATP in the stopped-flow. (Pre-mixing concentrations are stated in *C* and *D*.) The transients were fitted by three exponentials. Fitted rate constants of the phases are as follows: at 0.5 μM ADP, 120 s^{-1} (69% fractional amplitude), 12 s^{-1} (17%), and 1.3 s^{-1} (14%); at 2 μM ADP, 200 s^{-1} (46%), 15 s^{-1} (35%), and 1.5 s^{-1} (19%); at 50 μM ADP, first phase absent, 7.4 s^{-1} (76%), 0.87 s^{-1} (24%). Traces are offset for clarity. *D*, dependence of the fractional amplitudes of the first (*squares*), second (*solid circles*), and third (*open circles*) phases in the experiments of Fig. 5*C* on ADP concentration. Hyperbolic fits to the first and second phase amplitudes yielded ADP binding K_d values of 2.7 and 2.1 μM, respectively, in the experiment shown. Conditions were as in Fig. 2.

see also "Discussion"). The k_{obs} of the first phase increased steeply with ATP concentration (initial slope delineating $K_1'k_2' = 1.3 \pm 0.1$ μM^{-1} s^{-1}, Fig. 5*B*; TABLE TWO) and showed signs of saturation above 400 s^{-1} (k_2', Fig. 5*B*). The second phase k_{obs} also increased with increasing actin concentration and showed an initial slope about four times lower than that of the first phase (0.31 ± 0.08 μM^{-1} s^{-1}, Fig. 5*B*; TABLE TWO). The records contained an additional minor third phase with a k_{obs} of 1.0 ± 0.5 s^{-1}, which did not change with ATP concentration (data not shown). The fractional amplitudes of the three phases (phase 1, 46 ± 12%; phase 2, 36 ± 8%; and phase 3, 18 ± 4%) did not show a systematic dependence on ATP concentration.

The experiments above assessed ATP binding to a nucleotide-free pyrene-acto-mVIIB-S1 complex. We investigated the effect of ADP on this process by preincubating pyrene-acto-mVIIB-S1 with different concentrations of ADP, and by mixing these pre-mixtures with a large excess of ATP (250 μM post-mix) in the stopped-flow. These experiments also produced triphasic pyrene fluorescence transients. However, the k_{obs} values of the three phases remained constant with increasing ADP concentration (phase 1, 150 ± 40 s^{-1}; phase 2, 9.8 ± 3.5 s^{-1}; and phase 3, 1.2 ± 0.2 s^{-1}) (Fig. 5*C*). The fractional amplitudes of phases 1 and 2 flipped over in a hyperbolic manner (with phase 1 amplitude decreasing and phase 2 amplitude increasing) with increasing ADP con-

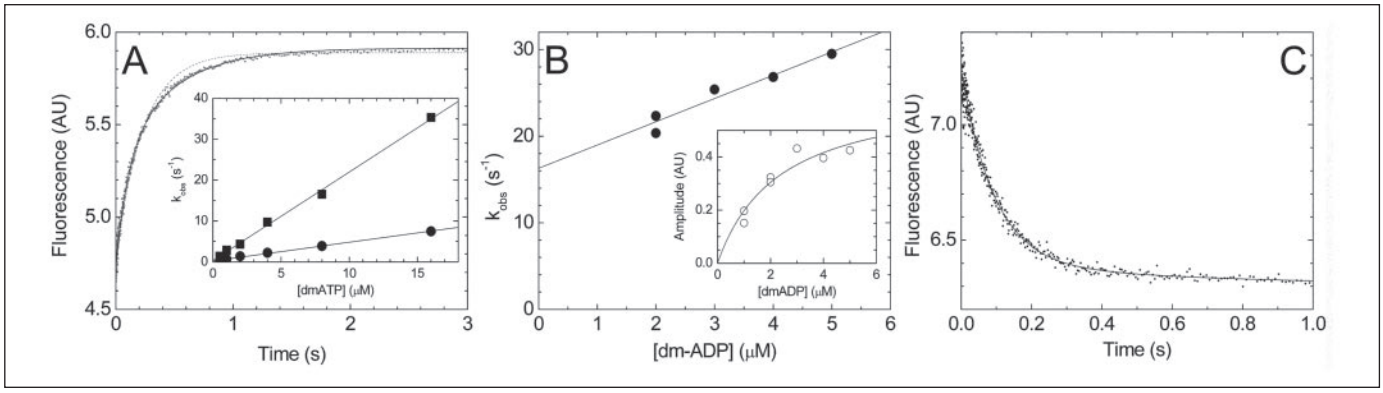

FIGURE 6. **Interaction of acto-mVIIB-S1 with dmATP and dmADP.** *A,* dmATP fluorescence transient obtained on rapidly mixing a pre-mixture of 0.1 μM mVIIB-S1 and 0.2 μM actin with 4 μM dmATP. A double exponential fit to the data yielded k_{obs} values of 9.7 s^{-1} (45% fractional amplitude) and 2.2 s^{-1} (55%). A single exponential fit (shown as a *dashed line*) showed systematic deviation from the experimental data. The *inset* shows the dependence of the k_{obs} of the first (*squares*) and second (*circles*) phases on dmATP concentration. Linear fits to the data sets gave second-order ATP binding rate constants ($K_1'k_2'$) of 2.2 ± 0.1 and 0.46 ± 0.02 μM^{-1} s^{-1} for the first and second phases, respectively. *B,* k_{obs} values of the single exponential dmADP fluorescence transients obtained on mixing a pre-mixture of 0.2 μM actin and 0.1 μM mVIIB-S1 with the indicated dmADP concentrations in the stopped-flow. The slope of a linear fit to the data set yielded a second-order binding rate constant of dmADP to acto-mVIIB-S1 of 2.7 ± 0.4 μM^{-1} s^{-1}, whereas the intercept of the plot delineated a dissociation rate constant of 16 ± 1 s^{-1}. The *inset* shows the dependence of the amplitude of the same transients on dmADP concentration. A hyperbolic fit to the data gave K_d of 2.7 ± 0.4 μM. *C,* dmADP fluorescence transient recorded on mixing a pre-mixture of 10 μM actin, 0.5 μM mVIIB-S1, and 10 μM dmADP with excess (1 mM) ATP in the stopped-flow. The data were fitted by a single exponential with a k_{obs} of 11 s^{-1} and an additional small linear decrease. Conditions were as in Fig. 2.

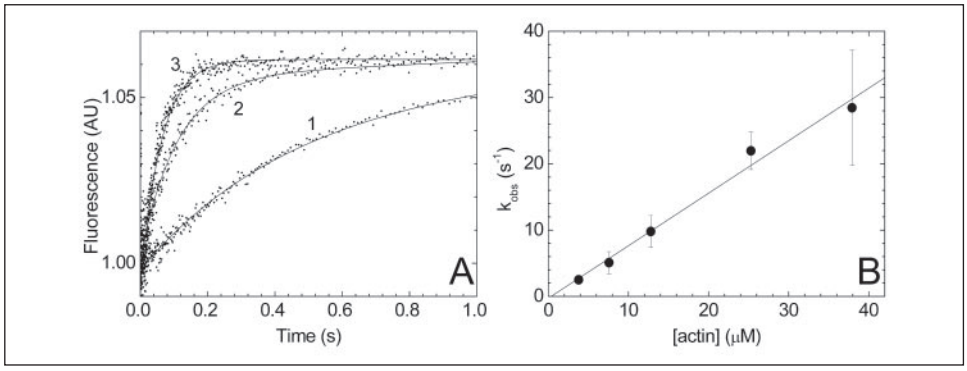

FIGURE 7. **Phosphate release from the acto-mVIIB-S1-products complex.** *A,* MDCC-PBP fluorescence records obtained in double-mixing stopped-flow experiments in which 1.6 μM mVIIB-S1 was first mixed with substoichiometric ATP (1 μM), incubated for 1 s for ATP binding and hydrolysis to occur, and then rapidly mixed with actin at various concentrations to accelerate product release. Fitted k_{obs} values of the traces shown are as follows: *trace 1* (3.8 μM actin) and 2.2 s^{-1}; *trace 2* (13 μM actin), 9.0 s^{-1}; *trace 3* (25 μM actin), 16 s^{-1}. *B,* dependence of k_{obs} in the experiments of *A* on actin concentration. A linear fit to the data had a slope (k_4'/K_9) of 0.79 ± 0.05 μM^{-1} s^{-1}. Conditions were as in Fig. 2 except that the KCl concentration was 10 mM.

centration, indicating an ADP dissociation constant (K_5') of 1.7 ± 0.9 μM (Fig. 5*D*; TABLE ONE). The fractional amplitude of phase 3 (0.21 ± 0.03) remained constant over the ADP concentration range examined.

The binding of dmATP to nucleotide-free acto-mVIIB-S1 under pseudo-first-order conditions was also multiphasic. This finding is again unusual in myosins and is in line with the pyrene-actin results discussed above. Upon mixing acto-mVIIB-S1 with dmATP under pseudo-first-order conditions in the stopped-flow, two exponential phases of dmATP fluorescence increase were observed throughout the examined dmATP concentration range (Fig. 6*A*). The two phases had roughly equal fractional amplitudes (phase 1, 0.46 ± 0.06; phase 2, 0.54 ± 0.06, TABLE TWO), which did not change with dmATP concentration. The k_{obs} values of both phases showed linear dependences on dmATP concentration with slopes of 2.2 ± 0.1 μM^{-1} s^{-1} (phase 1) and 0.46 ± 0.02 μM^{-1} s^{-1} (phase 2) (Fig. 6*A, inset*; TABLE TWO).

The binding of dmADP to acto-mVIIB-S1 was monophasic. The dependence of the k_{obs} values of the binding transients on dmADP concentration delineated a linear slope (k_{-5}') of 2.7 ± 0.4 μM^{-1} s^{-1} and an intercept (k_5') of 16 ± 1 s^{-1} (Fig. 6*B*; TABLE ONE). The absolute amplitude of the transients depended hyperbolically on dmADP concentration and indicated a dissociation constant (K_5') of 2.7 ± 0.4 μM (Fig. 6*B, inset*). The dmADP release rate constant (k_5') was also measured in a chasing experiment in which the acto-mVIIB-S1·dmADP ternary complex was mixed with a large excess of ATP (Fig. 6*C*). The single exponential dmADP dissociation transients delineated a k_5' of 9.6 ± 1.3 s^{-1} in these experiments (TABLE ONE).

Phosphate Release—We measured P_i release using MDCC-PBP, a fluorescently labeled phosphate-binding protein (22, 28). In double-mixing stopped-flow experiments, mVIIB-S1 was first rapidly mixed with sub-stoichiometric amounts of ATP (single turnover conditions), incubated for 1 s for ATP binding and hydrolysis to occur (*cf.* K_1k_2, and $k_3 + k_{-3}$ in TABLE ONE), and then rapidly mixed in the second mix with a range of actin concentrations to facilitate P_i release from the mVIIB-S1-products complex (28). After the first mix, an equilibrium mixture of the pre- and post-hydrolysis species will form (M·ATP and M·ADP·P_i in Scheme 1). The P_i release transients obtained under these conditions reflect two processes. First, the binding of M·ADP·P_i to actin (K_9) and subsequent P_i release (k_4') will result in a phase whose k_{obs} is expected to depend hyperbolically on actin concentration (Fig. 7, *A* and *B*). Second, if M·ATP is present at a significant concentration in the pre-mixture before the actin mix (*i.e.* K_3 is fairly reversible), then an additional slow phase will appear that results from the flux of the reaction through the pathway involving a possible slow actin-associated ATP hydrolysis (K_8 and k_3') (28). This phase was not significant in our experiments, in line with the quenched-flow and tryptophan fluorescence results showing that K_3 is fairly high and the cleavage step is rapid

($k_3 + k_{-3} = 160 \pm 30\ s^{-1}$) (Fig. 2, *B–C*; TABLE ONE). (A slow phase with a k_{obs} around 0.03 s^{-1} was present in all traces, but with control measurements we established that this phase was present also in the absence of mVIIB-S1 (data not shown).)

The fast phase k_{obs} increased roughly linearly with actin concentration in the examined range (up to 38 μM actin after the second mix) (Fig. 7, *A* and *B*). This indicates that the actin affinity of M·ADP·P_i is low ($K_9 > 40\ \mu M$), and only a lower limit of k_4' ($> 40\ s^{-1}$) can be determined. The linear slope of the plot of k_{obs} *versus* actin concentration gave an apparent second-order binding constant of M·ADP·P_i binding to actin (k_4'/K_9, *cf.* Scheme 1) of 0.79 $\mu M^{-1}\ s^{-1}$ (TABLE ONE).

DISCUSSION

mVIIB-S1 Exhibits a High Duty Ratio—Our detailed kinetic analysis shows that at high ATP and actin concentrations, the ADP release step from actomyosin is the single predominant rate-limiting step in the acto-mVIIB-S1 ATPase cycle (TABLE ONE; Scheme 1). All other steps including P_i release occur at least four times faster than the maximal steady-state ATPase rate. The duty ratio, *i.e.* the fractional abundance of the strong actin-binding states (predominantly the actomyosin·ADP state), calculated from the lower boundary of the maximal P_i release rate constant ($k_4' > 40\ s^{-1}$, entry into the strong binding state) and the ADP release rate constant ($k_5' = 10\ s^{-1}$, exit from the strong binding state) will be at least 80% ($= k_4'/(k_4' + k_5')$), similarly to other high duty ratio motors such as myosin V and VI (29, 30). The ATP hydrolysis equilibrium (K_3) is poised toward the M·ADP·P_i state in mVIIB-S1, which greatly contributes to a fast effective rate of P_i release, unlike in many other myosins including myosin II (18, 28, 31, 32), myosin X (19), and *Drosophila* myosin V (33) in which a more balanced kinetic partitioning between weak actin-binding states (AM·ATP, AM·ADP·P_i) lowers the duty ratio. This partitioning results in a non-negligible steady-state abundance of the weak actin binding states even in the case of mVIIB-S1, which is reflected in the fact that the steady-state V_{max}/K_{ATPase} ratio (0.22 $\mu M^{-1}\ s^{-1}$, Fig. 3; TABLE ONE) is remarkably lower than the apparent second-order rate constant of the binding of the M·ADP·P_i products complex to actin ($k_4'/K_9 = 0.79\ \mu M^{-1}\ s^{-1}$, Fig. 7*B*; TABLE ONE).

Kinetics of ATP-induced Actomyosin Dissociation Reveals Heterogeneity of Acto-mVIIB-S1 Complexes—In the ATP-induced acto-mVIIB-S1 dissociation transients, two ATP concentration-dependent phases could clearly be resolved throughout the examined ATP concentration range (Fig. 5, *A* and *B*; TABLE TWO). Because the k_{obs} values of both phases showed linear dependences on ATP concentration with very little tendency to saturate and the two phases were present even at low ATP concentrations, we interpret this biphasicity as a result of a conformational heterogeneity of the acto-mVIIB-S1 rigor complex rather than arising from consecutive steps during the actomyosin dissociation process as was the case in mammalian myosin IB (34). Consistent with this, dmATP binding to acto-mVIIB-S1 was also biphasic (Fig. 6*A*). The acto-mVIIB-S1 samples were extensively pretreated with apyrase prior to the stopped-flow experiments, which excludes the possibility that the biphasicity would appear due to the presence of ADP contamination. The fact that the processes of dmADP binding to acto-mVIIB-S1 (Fig. 6*B*) and dmATP binding to mVIIB-S1 in the absence of actin (Fig. 1*A*) were monophasic shows that this phenomenon specifically affects the interaction of ATP (or dmATP) with acto-mVIIB-S1 (Fig. 5, *A* and *B*, and Fig. 6*A*), and is not a result of the presence of a damaged subpopulation in the mVIIB-S1 protein. The ratios of the fractional amplitudes of the fast and slow phases in the independent experiments utilizing pyrene-actin and dmATP signals were similar (1.3 and 0.9, respectively; TABLE TWO) and indicated a reversible equilibrium between the two acto-mVIIB-S1 conformations ($K \approx 1$) with different ATP binding properties. Furthermore, the ratios of the second-order nucleotide binding rate constants of the first and second phases in the pyrene-actin and dmATP experiments were also very similar (4.2 and 4.8, respectively; *cf.* TABLE TWO). The differences in the absolute values of these rate constants are likely because of the effects of the presence of the pyrenyl and methylanthranyloyl groups in the different experiments.

As indicated from the biphasicity of the records even at low ATP (or dmATP) concentrations (Fig. 5, *A* and *B*; Fig. 6*A*), the equilibrium between the two acto-mVIIB-S1 states in the absence of nucleotide is considerably slower than the maximal steady-state ATPase rate (interconversion rate constant $<1\ s^{-1}$), and thus it probably does not form a part of the main ATPase pathway, but its existence may bear important structural implications.

Thermodynamic Coupling of ADP and Actin Binding to mVIIB-S1—A number of recent studies have revealed that the thermodynamic coupling between actin and ADP binding to the myosin head varies widely among different myosin isoforms (for reviews see Refs. 35 and 36). The classically studied sarcomeric myosin IIs (skeletal, cardiac, and scallop striated muscle) and *Dictyostelium* myosin II show a strong negative coupling, *i.e.* actin binding to myosin weakens the ADP affinity at least 30-fold and vice versa. In contrast, many other myosins show low actin-ADP coupling, which is associated with high ADP affinities of actomyosin ($K_5' < 20\ \mu M$) and slow ADP release rate constants. The resulting long lifetime (>50 ms) and high steady-state abundance of the strong binding actomyosin·ADP state may play a role in the tension-bearing function of these myosins and is also important in the mechanism of processive stepping of myosins V and VI (29, 30, 37, 38). Similarly to myosin VI and non-muscle myosin II isoforms, the ADP release constant of mVIIB-S1 was unaffected by actin (TABLE ONE), which is an important determinant of the long lifetime of the actomyosin·ADP state and thus the high duty ratio (18, 30, 31). The equilibrium constants of actin and ADP binding also showed a lack of coupling between the two binding events (both K_5'/K_5 and K_{10}/K_6 were close to unity; see TABLE ONE).

Besides the rate constant of ADP release from actomyosin, the ratio of the rate constants of ATP and ADP binding to actomyosin is an important determinant of the product inhibition of the actomyosin ATPase cycle by ADP, which may have physiological relevance under some conditions, as this ratio is very low in some actomyosins (*i.e.* they preferably bind ADP) (18, 30, 31). Most interestingly, the binding rate constants of dmATP and dmADP to acto-mVIIB-S1 ($K_1k_2 = 2.2\ \mu M^{-1}\ s^{-1}$, $k_5' = 2.7\ \mu M^{-1}\ s^{-1}$) were much more similar to each other than those of the unlabeled nucleotides, in which case there was a 4.5-fold preference for ADP ($K_1k_2 = 1.3\ \mu M^{-1}\ s^{-1}$, $k_{-5} = 5.8\ \mu M^{-1}\ s^{-1}$ from pyrene-actin data, TABLES ONE and TWO). Together with the slow ADP release step, these data indicate that the steady-state ATPase activity of mVIIB-S1 will be effectively inhibited by ADP even at ADP/ATP ratios below unity, similarly to the findings of Inoue and Ikebe (15) on rat myosin VIIA. In rat myosin VIIA, however, high ATP concentrations (>1 mM) were necessary for saturation of the steady-state ATPase activity and *in vitro* actin gliding motility implying that ATP binding to actomyosin VIIA is rather slow, which is not the case in mVIIB-S1 (Fig. 5, *A* and *B*; Fig. 6; TABLE TWO).

Implications for Processivity and Roles in Intracellular Transport—Based on the kinetic features of mVIIB-S1 (high duty ratio, slow ADP release), it is possible that this myosin isoform exhibits vertebrate myosin V-like single molecule processive walking along actin filaments, provided that the heavy chains dimerize via the predicted coiled-coil segment or other domains of the tail region. In line with this, a melanosome

transport model for mouse myosin VIIA in retinal pigment epithelial cells has been proposed in which myosin VIIA binds to the melanosome via MyRIP and, in turn, Rab27a proteins (13). This binding architecture is similar to that described for mouse myosin Va in melanocytes (myosin Va-melanophilin-Rab27a-melanosome) (39, 40). Apart from single-molecule processivity, the high duty ratio of myosin VII may be generally necessary for contact and tension maintenance.

Acknowledgments—We thank Antoine F. Smith for expert technical assistance; Dr. Howard D. White for the generous gift of dmATP, dmADP, and MDCC-PBP; and Judit Tóth for Drosophila calmodulin and comments on the manuscript.

REFERENCES

1. Sellers, J. R. (1999) *Myosins*, 2nd Ed., Oxford University Press, New York
2. Baker, J. P., and Titus, M. A. (1997) *J. Mol. Biol.* **272,** 523–535
3. Gibson, F., Walsh, J., Mburu, P., Varela, A., Brown, K. A., Antonio, M., Beisel, K. W., Steel, K. P., and Brown, S. D. (1995) *Nature* **374,** 62–64
4. Hasson, T., Skowron, J. F., Gilbert, D. J., Avraham, K. B., Perry, W. L., Bement, W. M., Anderson, B. L., Sherr, E. H., Chen, Z. Y., Greene, L. A., Ward, D. C., Corey, D. P., Mooseker, M. S., Copeland, N. G., and Jenkins, N. A. (1996) *Genomics* **36,** 431–439
5. Kiehart, D. P., Franke, J. D., Chee, M. K., Montague, R. A., Chen, T. L., Roote, J., and Ashburner, M. (2004) *Genetics* **168,** 1337–1352
6. Tuxworth, R. I., Weber, I., Wessels, D., Addicks, G. C., Soll, D. R., Gerisch, G., and Titus, M. A. (2001) *Curr. Biol.* **11,** 318–329
7. Hasson, T. (1999) *Curr. Biol.* **9,** R838–R841
8. Titus, M. A. (1999) *Curr. Biol.* **9,** 1297–1303
9. Petit, C. (2001) *Annu. Rev. Genomics Hum. Genet.* **2,** 271–297
10. Self, T., Sobe, T., Copeland, N. G., Jenkins, N. A., Avraham, K. B., and Steel, K. P. (1999) *Dev. Biol.* **214,** 331–341
11. Todi, S. V., Franke, J. D., Kiehart, D. P., and Eberl, D. F. (2005) *Curr. Biol.* **15,** 862–868
12. Yamashita, R. A., Sellers, J. R., and Anderson, J. B. (2000) *J. Muscle Res. Cell Motil.* **21,** 491–505
13. El-Amraoui, A., Schonn, J. S., Kussel-Andermann, P., Blanchard, S., Desnos, C., Henry, J. P., Wolfrum, U., Darchen, F., and Petit, C. (2002) *EMBO Rep.* **3,** 463–470
14. Kussel-Andermann, P., El-Amraoui, A., Safieddine, S., Nouaille, S., Perfettini, I., Lecuit, M., Cossart, P., Wolfrum, U., and Petit, C. (2000) *EMBO J.* **19,** 6020–6029
15. Inoue, A., and Ikebe, M. (2003) *J. Biol. Chem.* **278,** 5478–5487
16. Udovichenko, I. P., Gibbs, D., and Williams, D. S. (2002) *J. Cell Sci.* **115,** 445–450
17. Wang, F., Harvey, E. V., Conti, M. A., Wei, D., and Sellers, J. R. (2000) *Biochemistry* **39,** 5555–5560
18. Wang, F., Kovacs, M., Hu, A., Limouze, J., Harvey, E. V., and Sellers, J. R. (2003) *J. Biol. Chem.* **278,** 27439–27448
19. Kovacs, M., Wang, F., and Sellers, J. R. (2005) *J. Biol. Chem.* **280,** 15071–15083
20. Spudich, J. A., and Watt, S. (1971) *J. Biol. Chem.* **246,** 4866–4871
21. Cooper, J. A., Walker, S. B., and Pollard, T. D. (1983) *J. Muscle Res. Cell Motil.* **4,** 253–262
22. Brune, M., Hunter, J. L., Corrie, J. E., and Webb, M. R. (1994) *Biochemistry* **33,** 8262–8271
23. Malnasi-Csizmadia, A., Kovacs, M., Woolley, R. J., Botchway, S. W., and Bagshaw, C. R. (2001) *J. Biol. Chem.* **276,** 19483–19490
24. Park, S., and Burghardt, T. P. (2000) *Biochemistry* **39,** 11732–11741
25. Yengo, C. M., Chrin, L. R., Rovner, A. S., and Berger, C. L. (2000) *J. Biol. Chem.* **275,** 25481–25487
26. Criddle, A. H., Geeves, M. A., and Jeffries, T. (1985) *Biochem. J.* **232,** 343–349
27. Kouyama, T., and Mihashi, K. (1981) *Eur. J. Biochem.* **114,** 33–38
28. White, H. D., Belknap, B., and Webb, M. R. (1997) *Biochemistry* **36,** 11828–11836
29. De La Cruz, E. M., Wells, A. L., Rosenfeld, S. S., Ostap, E. M., and Sweeney, H. L. (1999) *Proc. Natl. Acad. Sci. U. S. A.* **96,** 13726–13731
30. De La Cruz, E. M., Ostap, E. M., and Sweeney, H. L. (2001) *J. Biol. Chem.* **276,** 32373–32381
31. Kovacs, M., Wang, F., Hu, A., Zhang, Y., and Sellers, J. R. (2003) *J. Biol. Chem.* **278,** 38132–38140
32. Kovacs, M., Toth, J., Nyitray, L., and Sellers, J. R. (2004) *Biochemistry* **43,** 4219–4226
33. Toth, J., Kovacs, M., Wang, F., Nyitray, L., and Sellers, J. R. (2005) *J. Biol. Chem.* **280,** 30594–30603
34. Geeves, M. A., Perreault-Micale, C., and Coluccio, L. M. (2000) *J. Biol. Chem.* **275,** 21624–21630
35. De La Cruz, E. M., and Ostap, E. M. (2004) *Curr. Opin. Cell Biol.* **16,** 61–67
36. Nyitrai, M., and Geeves, M. A. (2004) *Philos. Trans. R. Soc. Lond. B. Biol. Sci.* **359,** 1867–1877
37. Baker, J. E., Krementsova, E. B., Kennedy, G. G., Armstrong, A., Trybus, K. M., and Warshaw, D. M. (2004) *Proc. Natl. Acad. Sci. U. S. A.* **101,** 5542–5546
38. Rosenfeld, S. S., and Sweeney, H. L. (2004) *J. Biol. Chem.* **279,** 40100–40111
39. Wu, X., Wang, F., Rao, K., Sellers, J. R., and Hammer, J. A., III (2002) *Mol. Biol. Cell* **13,** 1735–1749
40. Wu, X. S., Rao, K., Zhang, H., Wang, F., Sellers, J. R., Matesic, L. E., Copeland, N. G., Jenkins, N. A., and Hammer, J. A., III (2002) *Nat. Cell Biol.* **4,** 271–278
41. Yengo, C. M., and Sweeney, H. L. (2004) *Biochemistry* **43,** 2605–2612